Vibrational spectroscopic study of pH dependent solvation at a Ge(100)-water interface during an electrode potential triggered surface termination transition

Fang Niu, Martin Rabe, Simantini Nayak, and Andreas Erbe

Citation: The Journal of Chemical Physics **148**, 222824 (2018); doi: 10.1063/1.5018796
View online: https://doi.org/10.1063/1.5018796
View Table of Contents: http://aip.scitation.org/toc/jcp/148/22
Published by the American Institute of Physics

Vibrational spectroscopic study of pH dependent solvation at a Ge(100)-water interface during an electrode potential triggered surface termination transition

Fang Niu,[1] Martin Rabe,[1] Simantini Nayak,[1] and Andreas Erbe[1,2,a)]
[1]*Max-Planck-Institut für Eisenforschung GmbH, Max-Planck-Str. 1, 40237 Düsseldorf, Germany*
[2]*Department of Materials Science and Engineering, NTNU, Norwegian University of Science and Technology, 7491 Trondheim, Norway*

(Received 9 December 2017; accepted 15 March 2018; published online 4 April 2018)

The charge-dependent structure of interfacial water at the n-Ge(100)-aqueous perchlorate interface was studied by controlling the electrode potential. Specifically, a joint attenuated total reflection infrared spectroscopy and electrochemical experiment was used in 0.1M $NaClO_4$ at pH ≈ 1–10. The germanium surface transformation to an H-terminated surface followed the thermodynamic Nernstian pH dependence and was observed throughout the entire pH range. A singular value decomposition-based spectra deconvolution technique coupled to a sigmoidal transition model for the potential dependence of the main components in the spectra shows the surface transformation to be a two-stage process. The first stage was observed together with the first appearance of Ge–H stretching modes in the spectra and is attributed to the formation of a mixed surface termination. This transition was reversible. The second stage occurs at potentials ≈0.1–0.3 V negative of the first one, shows a hysteresis in potential, and is attributed to the formation of a surface with maximum Ge–H coverage. During the surface transformation, the surface becomes hydrophobic, and an effective desolvation layer, a "hydrophobic gap," developed with a thickness ≈1–3 Å. The largest thickness was observed near neutral pH. Interfacial water IR spectra show a loss of strongly hydrogen-bound water molecules compared to bulk water after the surface transformation, and the appearance of "free," non-hydrogen bound OH groups, throughout the entire pH range. Near neutral pH at negative electrode potentials, large changes at wavenumbers below 1000 cm^{-1} were observed. Librational modes of water contribute to the observed changes, indicating large changes in the water structure. *Published by AIP Publishing.*
https://doi.org/10.1063/1.5018796

I. INTRODUCTION

Ions at aqueous charged solid-liquid interfaces are involved in various processes, e.g., corrosion, adhesion, lubricant friction, and drug release. As a result, the understanding of how anions and cations interact with water molecules in an electric field can contribute significantly to the elucidation of solvation at interfaces. The presence of dissolved ions leads to a rearrangement of water dipoles in the hydration shell structure in the vicinity of the interface.[1,2] This tendency of water to form "solvation shells" around ions offers key control over the nature and rates of chemical reactions in aqueous solutions.[3] Since any interaction among the ions is accompanied by a change on the water bonding, both adsorbed ions and water molecules are important at interfaces. This issue has been discussed in theoretical studies;[4–11] however, experimental difficulties exist in precisely controlling of the interactions between substances. The control of the electrode potential of a conducting solid may offer a certain level of control. One may even see the interface as a "large ion," the charge of which can be controlled.

The crystalline compound semiconductors germanium and silicon are widely used in the semiconductor industry and in nanotechnology.[12] Semiconducting oxides are of great importance in geology,[13] as additives in electrocatalysis,[14,15] and in passivating metallic materials.[16] Germanium has in early studies been suggested as a suitable model system for passive films on semiconductors.[17] Germanium also possesses an interesting feature that allows the control of the hydration shells with electrode potential: the germanium surface transforms from hydrophilic, OH-terminated to hydrophobic, H-terminated, when the applied electrode potential is sufficiently negative.[18–21] This surface transformation was so far investigated in acidic solution.[18,21,22] During the surface transformation, an intermediate surface state with both H and OH surface groups was inferred from a detailed analysis of the Ge–H stretching modes in between the initial OH-terminated state and the final H-terminated state.[21]

Some authors treat liquid water at a solid-liquid and gas-liquid interface as a separate thermodynamic system from bulk water.[23] This interfacial water phase was investigated using x-ray reflectivity,[24–26] vibrational sum frequency generation (SFG) spectroscopy,[27,28] and atomic force microscopy.[29,30] Vibrational spectroscopy in particular has been used to distinguish water in different states of hydrogen bonding.[31] In

[a)]E-mail: http://water-on-Ge100-pH@the-passivists.org.

addition to the most widely known and thermodynamically stable hydrogen bonding state of two to three hydrogen bonds per molecule,[32–34] the tetrahedral clustering in which one water molecule forms four hydrogen bonds is also possible locally in liquid state at interfaces.[35–38] Furthermore, at a hydrophobic surface, the lack of hydrogen bonding between water molecules often leads to the existence of the dangling OH bonds.[33,39–41] The possibility to switch the surface back and forth between these states makes germanium an attractive model system.[42]

The above-mentioned surface transformation on germanium also has huge consequences for the interfacial solvation shell; changes can be triggered by the electrode potential.[42] In perchloric acid, an acid which in electrochemistry is considered to have an only weakly adsorbing counterion, it was observed that interfacial water molecules were displaced from the Ge(100) surface by ≈1.9 Å at electrode potentials at which the surface was completely H-terminated.[42] The interfacial water possesses a different vibrational spectrum compared with bulk water, with the presence of dangling OH groups in contact with the H-terminated surface. In this work, the dependence of the interfacial water spectrum and water displacement as a function of electrode potential and hence surface charge was investigated by electrochemistry-coupled attenuated total internal reflection infrared (ATR-IR) spectroscopy over a pH range ≈1–10, i.e., covering the acidic to slightly alkaline range, all in the perchlorate-based electrolyte. Water vibrational spectra were analyzed in detail by means of a deconvolution method based on singular value decomposition (SVD) of the potential-dependent spectra, which was previously applied to study transitions between peptides with different secondary structures.[43] This approach provides information on the desolvation of a germanium electrode during the surface transformation and the interfacial water bonding patterns.

II. MATERIALS AND METHODS

A. Electrochemical spectroscopic experiments

All electrolytes used in this work have a ClO_4^- concentration of 0.1M and were prepared based on $NaClO_4$ or a mixture of $NaClO_4$ and $HClO_4$, with pH adjusted by addition of NaOH. Electrolytes were freshly prepared before experiments. All the solutions were purged with Ar prior to the experiment, and the gas space above the electrolyte in the electrochemical cell was purged continuously with Ar during the experiment. The ambient temperature for all experiments was (23 ± 2) °C.

Double side polished trapezoidal Sb-doped n-type Ge(100) (crystal GmbH) of size 52 mm × 20 mm × 2 mm, with an angle of incidence of 60° and hence 13 internal reflections was applied as working electrode internal reflection element (IRE). The orientation of the bulk crystal was confirmed by x-ray diffraction. An electrochemical ATR-IR setup was used as described earlier,[42,44,45] inside the sample chamber of a Vertex 70v Fourier transform IR spectrometer (Bruker). The IRE area in contact with the solution was approximately 24 mm × 17 mm ≈ 4 cm^2, yielding ≈7 effective reflections probing the solution. A double junction Ag/AgCl/3M KCl microreference electrode (World Precision Instruments) was used as the reference electrode, and a platinum foil (99.99%, 1.2 cm × 1 cm) was used as the counter electrode. All electrode potentials E in this work were reported with reference to the standard hydrogen electrode (SHE). IR spectra with p-polarized light were recorded using a middle band mercury cadmium telluride (MCT) detector. Each spectrum was accumulated over 400 scans and displayed as the absorbance $A = -\log_{10}\left(\frac{I_S}{I_0}\right)$, of which the intensity I_s detected in a certain sample state was divided by the reference spectrum intensity I_0. I_s was measured in a potential range from 0.21 V to −0.79 V in steps of 0.1 V, first in the direction of decreasing potential and then backward in the direction of increasing potential. Immediately after measurement of each I_s, a corresponding reference spectrum I_0 was measured at a fixed potential of 0.21 V. For the calculation of each absorbance spectrum, its corresponding reference spectrum was used, to avoid effects of drift from the MCT detector. Every series of experiments was carried out at least three times. The experiments at pH ≈ 6 were carried out five times.

Electrochemical experiments were performed using an Iviumstat potentiostat (Ivium). During ATR-IR experiments, electrode potential was controlled during the spectra acquisition with a simultaneous recording of currents in the chronoamperometry mode. Before each electrochemical ATR-IR experiment, cleaning of the germanium surface was conducted by 20 cyclic voltammogram (CV) cycles in the range of 0.21 V to −0.89 V. Dedicated CVs shown here were recorded in a separate series of experiments in a classical electrochemical glass cell with an Ag/AgCl/3M KCl reference electrode which was in contact with the electrolyte by a Luggin capillary and a gold counter electrode (approximately 1 cm × 1 cm). Peak centers for reductive CV peaks were determined by reading the minimum of the current after subtraction of a linear baseline. Note that the fresh preparation of different electrolytes leads to some differences in pH between measurements of the CV discussed in the manuscript and of the ATR-IR spectra. Absorbance spectra and CVs from the main experimental series are available as raw data online.[46]

B. Singular value decomposition (SVD)-based deconvolution

Electrode potential dependent spectra in the OH stretching mode region were analyzed by means of a SVD-based deconvolution routine.[47,48] First, individual linear baselines were subtracted from the spectra. Baselines were determined by the absorbances at wavenumbers $\tilde{\nu}$ of 2400 cm^{-1} and 3850 cm^{-1}. Spectra at positive potentials without significant potential-dependent changes as well as spectral outliers were omitted. The spectra were ordered in the columns of data matrix $A(\tilde{\nu}, E)$. SVD was applied via the MatLab function svd(), yielding the three matrices U, S, and V^T, the transpose of V,

$$A(\tilde{\nu}, E) = USV^T, \tag{1}$$

with U containing basis spectra, S containing the singular values, and V containing the potential dependence of the

corresponding columns in U. After inspection of the singular values and the initial 4 columns in U and V, components above the rank of 3 were omitted since they contained mainly noise. To describe the spectra in A by means of overlapping transitions, it was assumed that

$$USV^{\mathrm{T}} = DF^{\mathrm{T}}, \tag{2}$$

with F containing potential-dependent sigmoidals of the single spectral components in D. Using the pseudoinverse of F^{T}, $F^{\mathrm{T+}}$, one obtains

$$D = USH \tag{3}$$

with

$$H = V^{\mathrm{T}}F^{\mathrm{T+}}. \tag{4}$$

The matrix H contains coefficients that determine how the weighted basis spectra US are mixed to yield the single spectral components in D. These coefficients were determined by fitting the columns in V. A matrix F whose columns $f(E)_i$ contain one sigmoidal transition per spectral component in D was constructed as

$$f(E)_i = b_i + \frac{m_i - b_i}{1 + \exp\left(\frac{E_{\mathrm{m},i} - E}{\delta_i}\right)}. \tag{5}$$

Here the subscript i denotes the ith transition as column in F, b is the minimum value, m is the maximum value, δ is the broadness, and E_{m} is the midpoint of the transition. The function ϕ to be minimized by a nonlinear least square algorithm was[47]

$$\phi = S(V^{\mathrm{T}} - V^{\mathrm{T}}F^{\mathrm{T+}}F^{\mathrm{T}}). \tag{6}$$

The single spectral components D were determined from Eqs. (3) and (4).

For the data presented here, 3 components in F were in most cases sufficient to describe the main features in the spectra, as was assessed by a comparison of the reconstruction DF^{T} with the original data $A(\tilde{\nu}, E)$. Two different sorts of components were identified: (I) One base spectrum that represents the spectra with low absorbance at potentials close to the reference potential. This spectral component has an F component that is a constant baseline or a single step function. It was fitted by setting the parameter b constant to 0.5 and E_{m} was below the minimal measured potential in the case of a linear baseline or close to the highest measured potential in the case of a step function. (II) Difference spectra with a sigmoidal shape in F. For these, b was set constant to 0 and E_{m} was left to vary freely. For all components, $\delta < 0$ was left to vary freely, and $m = 1$.

III. RESULTS AND DISCUSSION

A. *In situ* spectroelectrochemical investigations

In acidic electrolytes, it was observed that at sufficiently negative electrode potentials, $E \lesssim -0.2$ V, the germanium surface transforms to an H-terminated surface.[18,19,22] CVs on Ge(100) in perchlorate electrolytes of different pHs are shown in Fig. 1. The CV at the most acidic pH in an Ar saturated electrolyte is consistent with previously published CVs,[18,21] with an anodic peak assigned to the formation of an oxide,[18,19,49] and a cathodic current peak assigned to the surface termination change to Ge–H. The appearance of the Ge–H absorbance in the ATR-IR spectra in Fig. 2 confirms the assignment of the reductive CV peak to a reductive surface transformation.

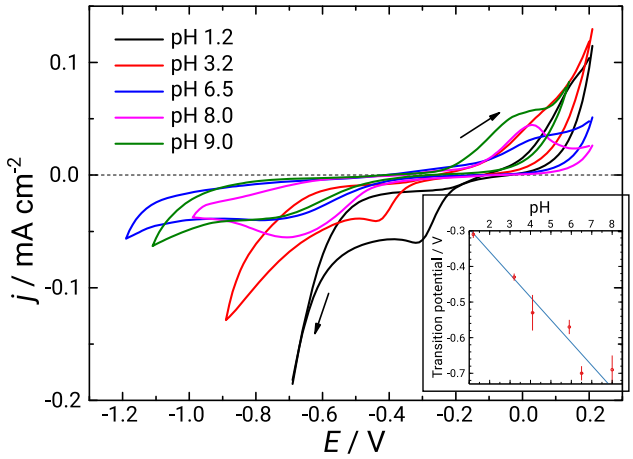

FIG. 1. CVs of Ge(100) in an Ar saturated 0.1M $NaClO_4$ electrolyte for different pH values as indicated in the graph, with a scan rate of 50 mV/s. Arrows indicate the scan direction. The horizontal dotted line indicates zero current. Inset: pH dependence of the potential with peak cathodic current, including linear fit.

The peak potential of the reductive surface transformation in the negative sweep was determined as a function of pH and is shown in Fig. 1 as an inset. At the most acidic pH, the peak was observed around −0.3 V. The slope of the pH dependence was obtained from the linear fit as −(59 ± 12) mV per pH unit. This value is within the experimental accuracy in agreement with the reported thermodynamically expected Nernst slope of 59.16 mV per pH unit change at 25°,[50] for the reaction

$$\mathrm{Ge{-}OH} + 2\mathrm{H^+} + 2\mathrm{e^-} \rightleftharpoons \mathrm{Ge{-}H} + \mathrm{H_2O}. \tag{7}$$

On the other hand, peak potentials of the oxidative peak show no systematic dependence on the pH. The CVs in acidic solution have been discussed in detail previously,[19,20,22] and this discussion shall not be taken up here, especially as far as the fine structure of the peaks is concerned. Lack of pH dependence of the anodic peak points to a lack of involvement of $2H^+$ in the oxidative process. Analysis of the electrochemical data is complicated by the slight solubility of germanium oxide.[51] The conclusion can only be that the anodic current peak cannot represent the counter reaction to the surface transformation discussed above. This work shall focus on the reductive surface transformation related to the cathodic peak.

Spectra at pH 1.4 have been discussed in a previous work in detail.[42] Therefore, focus here shall be on the pH-dependent differences in the spectra. The ATR-IR spectra at higher pH (Fig. 2) show a qualitatively similar trend as the spectra at pH 1.4.[42] The appearance of the mode at 1970 $\mathrm{cm^{-1}}$, assigned to a Ge–H stretching mode,[19,21,22] occurred at the same potential as the negative difference absorbance in the region of the OH stretching modes was observed. The appearance of this peak also shifts to negative potentials with increasing pH, confirming the expectations on the basis of the CVs.

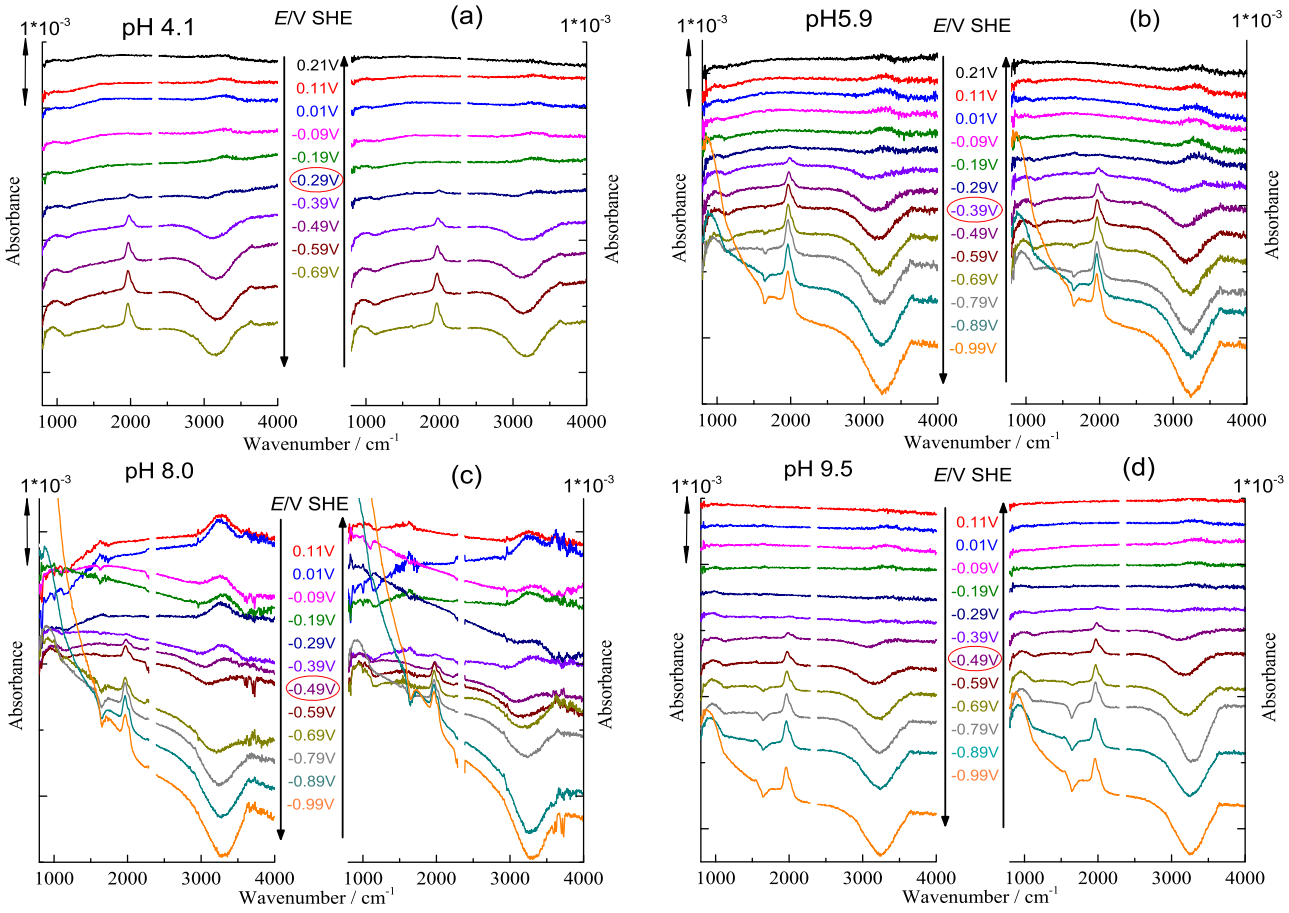

FIG. 2. ATR-IR absorbance spectra in p-polarization, on Ge(100) in Ar saturated 0.1M ClO_4^- at adjusted pH as indicated in the respective panel. The pHs in this figure are slightly different from those at which CVs were recorded in a classical electrochemical cell as shown in Fig. 1. Each panel presents data recorded in the direction of (left) decreasing and (right) increasing electrode potential. Respective potentials for the measurement are indicated in the middle of the graph. The onset potentials of the surface transformation have been labeled by a red ellipse. An absorbance scale is indicated near the respective axis. Spectra have been vertically offset for clarity. Raw data are available online.[46]

Figure 3 shows the Ge–H region of the spectra in detail. Besides the differences in onset potential, the evolution of the Ge–H region of the spectra is similar at all pH. At the more negative potentials, the peak consists of two components centered at 1965 cm^{-1} and 2025 cm^{-1}, assigned to stretching modes of $Ge–H_1$ and $Ge–H_2$ groups, respectively.[21,52–55] As discussed previously,[21] the peak shifts slightly after its initial appearance. There is no strong pH dependence of the internal structure and positions of the Ge–H stretching modes. Hence, these should not be discussed further in this work.

In the negative potential scan, the increase in negative difference absorbance of the ClO_4^- antisymmetric stretching mode at 1115 cm^{-1} (Fig. 2) indicates a repulsion of electrolyte ions from the surface.[44,56–58] The most striking change with pH in the spectra in Fig. 2 is the observation of positive shoulders below 1000 cm^{-1}. A strong increase of absorbance towards low wavenumbers could be related to free charge carrier absorption, as charges could accumulate near the interface during polarisation. Baselines in similar systems have been successfully described by models based on free carrier absorption.[22,59] From the internal structure of the baselines at pH 9.5 and −0.99 V as well as pH 8.0 and −0.89 V, it is obvious that the Drude-type absorption of free electrons cannot be the only cause for the observed baseline shift. Absorbance A in this case is supposed to scale with wavenumber $\tilde{\nu}$ as $A \sim \tilde{\nu}^{-2}$,[22,59,60] without peaks. (One could argue that the observed internal structure is in a region where the system approaches total absorption, hence making detection not reliable.) On the other hand, holes in germanium show characteristic absorptions at ≈3500 cm^{-1}, 2200 cm^{-1}, and 1800 cm^{-1},[61,62] which have been explained by transitions between three energy levels near the top of the valence band.[62,63] Two of these transitions have also been observed in germanium in contact with electrolyte.[59] The band at ≈ 1800 cm^{-1} has the strongest absorption coefficient.[61] In the spectra recorded here, none of these characteristic features has been observed. In addition, free carrier absorption is not supposed to depend strongly on the pH, however, the observed strong baseline shifts do. If the observed baseline changes were due to free carrier from charge accumulation near the interface, a correlation to the observed current may be expected. When comparing the spectra at wavenumbers below 1500 cm^{-1} at the different pHs, however, large absorption is observed at intermediate pH, irrespective of the current. In particular, at low pH, the effects on the baseline are much lower, even though the current is higher. Therefore, while free charge carrier absorption is likely to contribute to the spectra at low wavenumbers, it cannot be the only reason for the observed baselines. Surface oxide formation in the reference

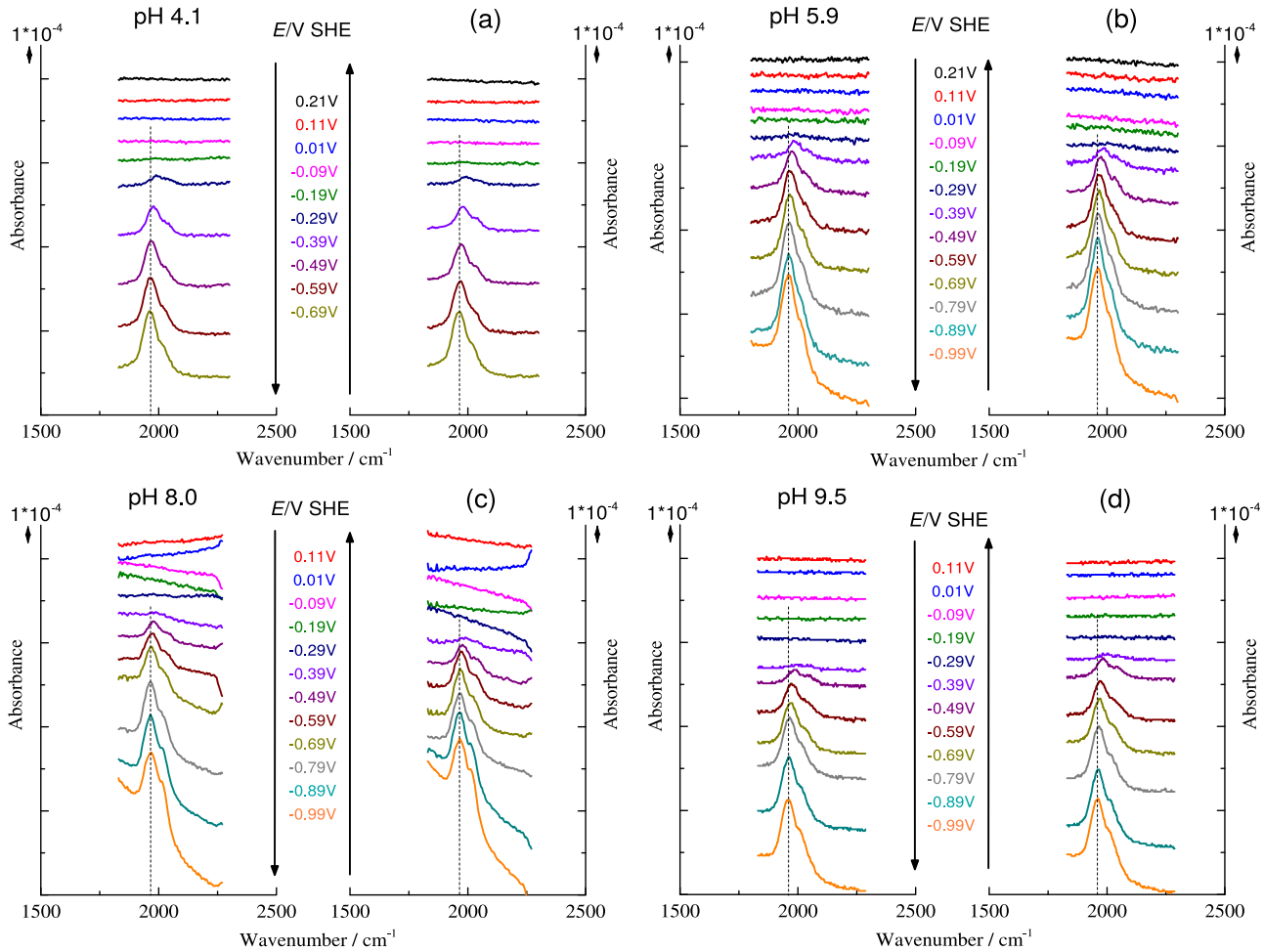

FIG. 3. Enlarged Ge–H stretching mode region of ATR-IR absorbance spectra from Fig. 2. Each panel presents data recorded in the direction of (left) decreasing and (right) increasing electrode potential. Respective potentials for the measurement are indicated in the middle of the respective panel. Dashed lines indicate the peak center at the most negative potentials. The difference absorbance of 10^{-4} is indicated by arrows next to the absorbance axis. Spectra have been vertically offset for clarity.

measurement may in part account for some features but can also not explain the overall shape of the spectra.

On the other hand, absorption spectra of water show a strong increase in absorbance below ≈1000 cm^{-1}[64,65] because of the onset of librational modes of water.[66,67] A simple way to evaluate if librational modes of water contribute to the baseline in this region is the use of an experiment in D_2O-based electrolytes. In D_2O, the onset of the librational modes shifts by ≈300 cm^{-1} to tower wavenumbers compared to H_2O.[68] Consequently, control experiments were conducted in which spectra in a D_2O-based electrolyte were compared to spectra recorded in an H_2O-based electrolyte. In this series, only a limited potential range was studied, and a different referencing scheme was used, all in order to limit the possibilities of D–H exchange. Results are shown in Fig. 4. The spectra in D_2O show a negative D_2O bending mode at ≈1200 cm^{-1},[68] and positive peak at ≈1100 cm^{-1}, assigned again to the antisymmetric ClO_4^- stretching mode. Importantly, the increase in the baseline observed in H_2O slightly below 1000 cm^{-1} is shifted at least by 100 cm^{-1} to lower wavenumbers, in line with an interpretation that librational modes do play a role here. The increased baselines observed in the main experimental series (Fig. 2) are therefore also interpreted as containing contributions of the librational modes of water. Because of the diverging penetration depth of the evanescent wave at low wavenumbers,[69] absorbance of bulk solution increases significantly with decreasing wavenumber, in line with the observations in the spectra. The magnitude of the observed differences cannot be explained by changes in solvation of the interface alone. Instead, they indicate that significant, potential induced changes of the solvation shell structure in the electrolyte in the interfacial region occur accompanied with the surface transformation at these pHs. As these features are observed in potentials where hydrogen evolution occurs, it is likely that the reaction products, OH^- ions, are present in the solution near the interface. The observed differences at these pHs may therefore be related to changes in interfacial pH. A detailed investigation of the region <1000 cm^{-1} requires measurements in the far-IR spectral range, which was not accessible in the setup used here. Consequently, no disentanglement of the contributions of free charge carrier absorption and librational modes was attempted in this work. Rather, the quantitative discussion from now on shall focus on the situation at the water bending and stretching mode region around 1650 and 3400 cm^{-1}, respectively, with stronger absorbance peaks, which also shows potential triggered changes related to

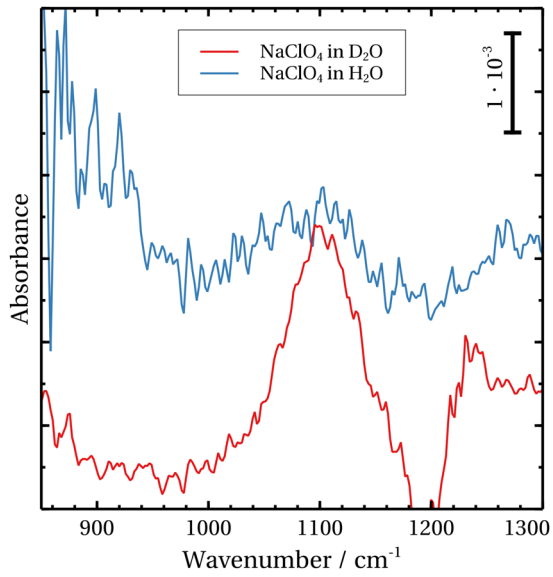

FIG. 4. Difference absorbance spectra between sample potential –0.49 V and reference potential –0.29 V in $NaClO_4$ in H_2O and D_2O at pH/pD ≈ 10.5.

the changes of orientation or quantity of water molecules near the surface.[65,70]

Two different effects contribute to the negative difference absorbance in the OH stretching mode region: the repulsion of water from the hydrophobic Ge–H surface and also the loss of surface-bound hydroxyl groups during the surface transformation. On the other hand, in the OH_2 bending mode region, the surface hydroxyl groups are expected to show a significantly shifted absorption peak compared to pure water. The absorbance in the bending mode region is, however, lower than in the stretching mode region, and at the same time, this regions is significantly affected from residual water vapor features in the spectra. Typically, the difference absorbance in the bending mode region is negative at the lowest potentials investigated, as expected from the analysis of the bending mode. Especially before the surface transformation, individual spectra show positive contributions. A consistent systematic quantitative analysis of these spectra was not possible. Overall, the observations are consistent with an interpretation of a two-stage transformation process. In the first stage, the loss of surface hydroxyl groups leads to the negative difference absorbance of the water stretching mode. After an intermediate state, possibly a mixed terminated surface,[21] the surface is mostly hydrogen terminated, making it hydrophobic. Qualitatively, this picture is similar for all pHs, with shifting transition potentials.

B. Structure of the Ge(100)/solution interface

Analysis of the spectra proceeded as introduced previously.[42] Briefly, from the negative difference absorbance in the OH stretching mode region, 2700–3700 cm^{-1}, an effective thickness of a "hydrophobic gap," i.e., a desolvated interfacial region with refractive index 1 was calculated. To do so, bulk optical constants of water were used,[64] in an own implementation of a matrix method,[71,72] in the framework of continuum electrodynamics, considering stratified structures only. Results are displayed for the different pHs in Fig. 5. Before analyzing the results, it should be made clear that the authors use the term "effective thickness" implying that this is not necessarily a homogeneous layer that forms at the interface. Rather, interfacial water is rearranged such that the first water layer is slightly displaced from the solid surface. The "effective thickness" corresponds to the thickness of a homogeneous gap which would show the same effect on the spectra as the actual rearrangement in the interfacial region. The results from this work do not permit any conclusions as to the internal structure of this layer. In particular, the effect of surface roughening on the spectra was not explicitly considered such that changes in roughness may enter the above described "effective thickness." The effect of roughening of the surface on local fields has previously been investigated for a germanium/water interface.[22] Absorbance enhancements were calculated to be <3 over a large range of geometries investigated, only extremely sharp structures yielded larger enhancements.[22] Neglecting roughening between the sample and respective reference measurement in the protocol used here will therefore still yield results in the correct order of magnitude. In addition, roughening on a length scale much smaller than the wavelength would lead to scattering of light, which is typically manifested in a baseline following the wavelength dependence of

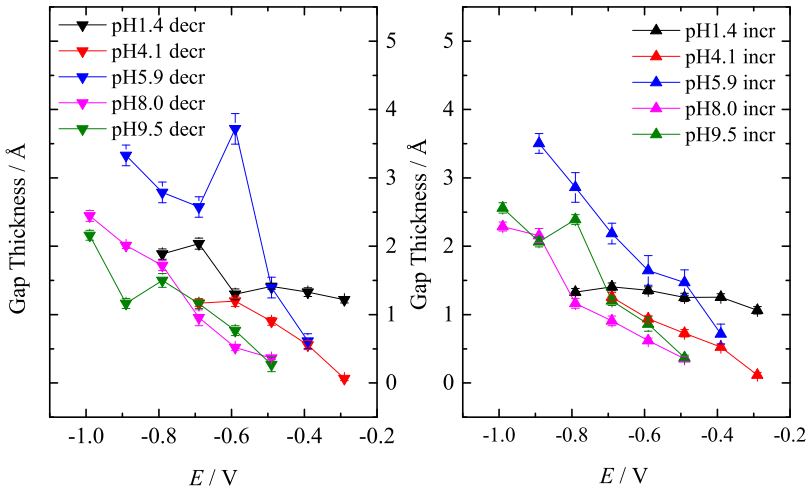

FIG. 5. Thickness of the hydrophobic gaps at the Ge(100)/solution interface as a function of electrode potential at different pHs as indicated in the graph. Both results recorded in the direction of decreasing ("decr") and increasing potential ("incr") are shown. The extremely high value at –0.5 V, pH 5.9, decreasing potential, may be regarded as an outlier.

Rayleigh scattering,[60] i.e., show a straight line decaying to lower wavenumbers. Enhanced absorption of light near sharp tips can only occur if significant field strength is scattered into the near field, which must consequently also reflect in the baseline. As such a baseline dependence is not observed, not even at high wavenumbers, scattering and surface enhancement cannot significantly affect the results obtained here. Even if individual surface features exist which increased absorbance in their vicinity, they are not present on the majority of the surface, and will thus not dominate the spectra.

The obtained effective gap thickness values are shown in Fig. 5 and are on the order of few Å. The gap thickness increases in the negative potential step direction and decreases in the reverse positive potential step direction. Another common feature observed is the pH dependence of the gap thickness. At the same applied potential, the maximum gap values are obtained near neutral pH. In other words, in the electrolyte of pH 5.9, the germanium surface was more hydrophobic at sufficiently negative potential than in the other electrolytes investigated. The extremely high thickness value of 3.7 Å at –0.59 V is regarded as an outlier.

In a next analysis step, the bulk water spectrum calculated for a layer of the thickness shown in Fig. 5 was subtracted from the experimentally obtained difference absorbance spectra (Fig. 2).[42] Thus obtained spectra shown in Fig. 6 represent the deviation of the interfacial water spectra from bulk water spectra. (In a previous work,[42] both the bending mode region and the stretching mode region of the spectrum were used to determine the effective gap thickness. The same analysis procedure was conducted once using the thickness values obtained from the bending mode region, and once using those from the stretching mode region. While the resulting spectra were quantitatively different, qualitative results remain unchanged. Because of the difficulties encountered here in the analysis of the bending mode region at some pHs, the bending mode region is not analyzed. The obtained difference spectra in Fig. 6 do therefore contain the effect of both OH from the surface termination above the transformation potential, as well as interfacial water. A large negative contribution is expected to originate from the surface-bound OH at positive potentials.) Notice that the balance between the observed positive or negative peaks is slightly modified if errors were made in the determination of the hydrophobic gap thickness; however, the overall shape of the spectra remains unchanged. In Fig. 6, the OH stretching mode region shows a split into three components: a negative component centering at 3060 cm^{-1}, a positive smaller component centering at 3440 cm^{-1}, and another positive sharp peak at 3640 cm^{-1} which is the smallest. The peak

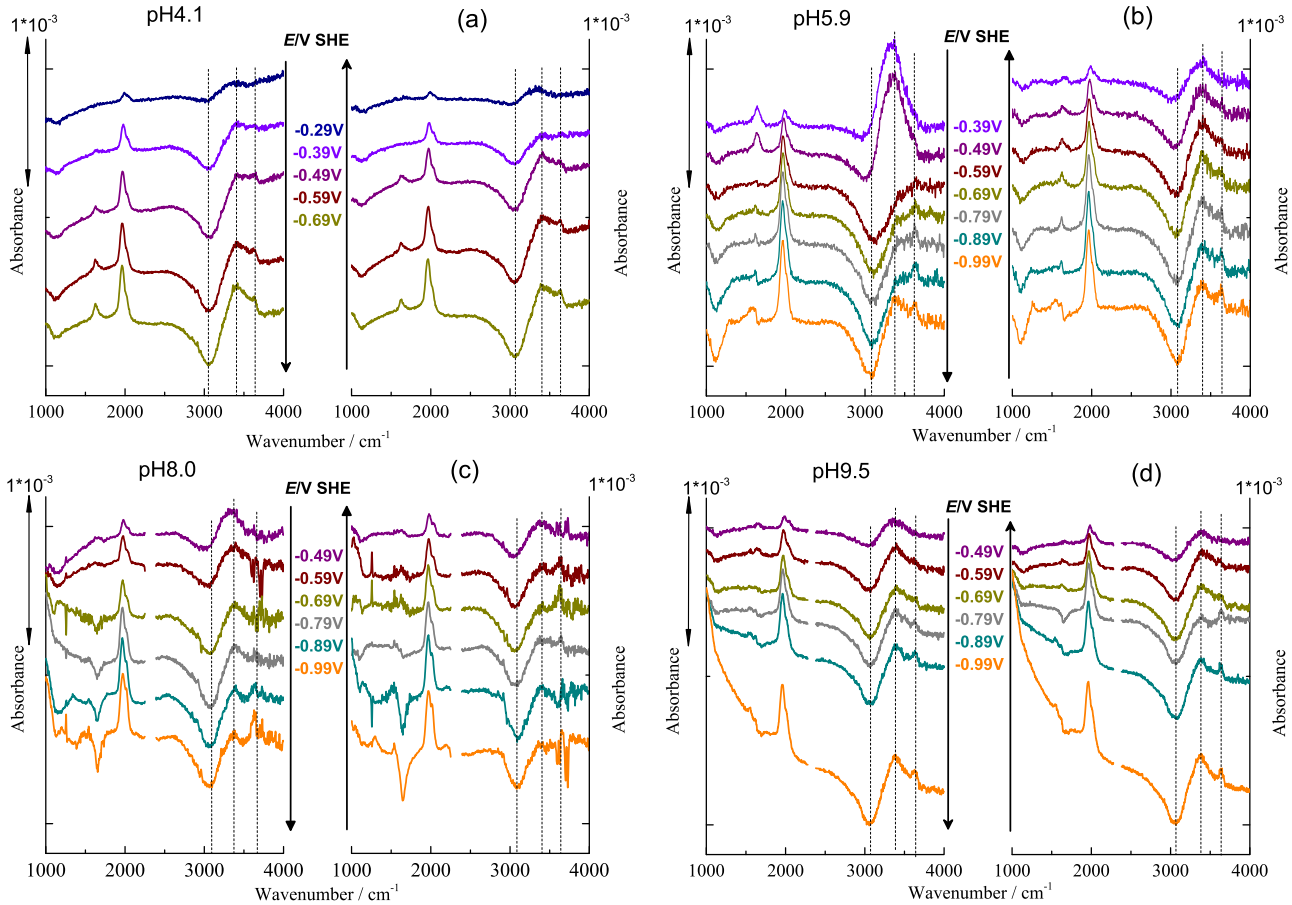

FIG. 6. ATR-IR difference absorbance spectra of interfacial water in 0.1M ClO_4^- adjusted to the respective pH at different electrode potentials. Spectra were obtained from subtraction of calculated spectra with bulk optical constants of water, separated from the germanium by a hydrophobic gap. Details of the method have been presented elsewhere.[42] Shown spectra thus represent the deviations of interfacial water from bulk water at the respective potential. An absorbance scale is shown near the respective axis. Spectra have been vertically offset for clarity.

located at 3060 cm^{-1} is attributed to water molecules with high degree of hydrogen bonding.[73–77] As this component is negative in this study, a loss of strongly hydrogen-bound water is observed at the Ge–H terminated surface. Other studies by simulations,[8,78] or SFG,[28,41] found water molecules in the strongly hydrogen-bound so-called "ice-like" structure at hydrophobic interfaces.

The absorbance peak at 3440 cm^{-1} is assigned to the water stretching modes which has a similar position to standard bulk hydrogen bonding pattern. At negative potentials, this peak is mostly slightly positive in this work, indicating an increase in water molecules in the average hydrogen bonding state compared to bulk water, independent of pH.

The slightly positive peak centering at 3640 cm^{-1} is only visible in a certain low potential region. (In some spectra, the residual water vapor features are also detectable. Since these features are not very strong, they can be distinguished from the peak at 3640 cm^{-1}.) This peak may be interpreted as originating from "free," dangling hydroxyl groups that are not involved in hydrogen bonding at the interface at potentials negative of the surface transformation. The existence of "free water" was detected previously by SFG at interfaces between water and hydrophobic liquids,[33,41,79–82] or during protein adsorption.[83,84]

The observed changes with potential in Fig. 6 are not fully reversible after reverting the potential stepping direction. The negative scan might lead us to a certain extend of surface defects, requiring a slightly different potential to trigger the surface transformation back. The hydrogen evolution reaction at low potentials and the consequent shift of pH near the interface in these unbuffered systems also likely affect the measured spectra.

C. SVD-based analysis of components in the OH stretching mode region

The potential dependence of the bands in the OH stretch region was studied in more detail by means of a SVD-based deconvolution. This linear algebraic method allows the identification of partially overlapping transitions and the corresponding overlapping spectral components in spectra depending on an external variable, amongst others in the IR.[43] The potential dependence of the spectral components was modeled by a sigmoidal function. Original difference absorbance spectra such as those shown in Fig. 2 were used as input for the procedure. The subtraction of the bulk water equivalent spectrum discussed in Sec. III B was not applied to the input spectra, and contributions from bulk water can therefore still be present in the resulting spectra. As an example for the results, the deconvolution of the spectra at pH 8 during the scan with decreasing potential is shown in Fig. 7. In this example, the procedure yielded the base spectrum in the F_3 and D_3 component. The base spectrum is the small spectral contribution close to the reference potential which does not change significantly during potential changes, which is evidenced by the according F_3 component which is constant over the potential range. The components F_1 and F_2 are actual sigmoidal transitions with their midpoints at ≈−670 mV and ≈−980 mV,

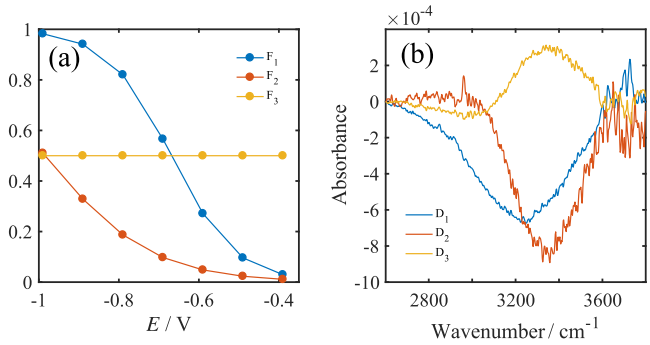

FIG. 7. Result of SVD-based deconvolution for spectra at pH = 8 recorded with decreasing potential. The original spectra are represented by DF^T according to Eqs. (1) and (2). (a) Components of F showing the potential dependence of the spectral component in D. (b) Components of D, representing the main spectral changes during potential decrease, multiplied by the respective component in F.

respectively. Their according spectral components D_1 and D_2 represent broad negative bands centered at ≈3240 cm^{-1} and ≈3350 cm^{-1}. Thus both transitions represent a step-wise decrease of absorbance in the OH band at the different potentials, resulting in the overall negative OH stretching mode band.

For all measured OH bands at the different pHs, a similar trend with potential was observed. The potential dependency could always be described by two well-separated spectral components that vary differently with potential. Figure 8 shows the pH dependence of the different components. The spectral component centered at the higher wavenumber ν_{high} always appears at lower potential, i.e., its E_m is smaller. The component at the lower frequency ν_{low} always has the higher E_m which shows a pH dependence that coincides with the pH dependence of the appearance of the Ge–H peak [Fig. 8(a)]. Based on the previous analysis of the potential dependence of the Ge–H stretching modes, the surface transformation (7) was argued indirectly to be a two-stage process.[21] The results obtained here are a direct confirmation of this previous interpretation and extends this to a large pH range. The component that appears first during decreasing electrode potential, i.e., ν_{high}, represents the initial loss of OH groups and associated change in surface solvation when the surface transformation sets in, presumably to a surface with mixed termination, containing both Ge–H and Ge–OH groups.[21] Consequently, the onset of this component coincides with the onset of the observation of the Ge–H mode. The component that sets in at more negative potentials shows a further loss in OH groups and surface solvation as the second stage of the transformation change, which finished with a completely H-terminated surface. It is worth noting that the component at more negative potentials is always higher in frequency. Therefore, the solvation shell lost in the first step contains water molecules with stronger hydrogen bonds, and while only weakly hydrogen-bound species are lost in the second stage. This behaviour is consistent with the above interpretation of a mixed surface intermediate, which is already partly Ge–H terminated and hence already more hydrophobic than the initial surface. It must be noted that the effects found in the SVD-based analysis contain both solvation related and

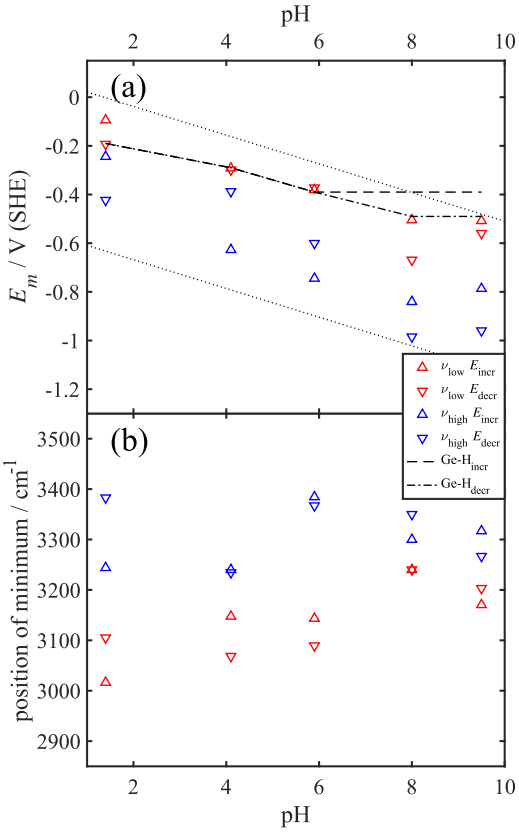

FIG. 8. Overview of results obtained from SVD-based deconvolution of potential-dependent spectra in the O–H stretch region. (a) Midpoints of transitions and first appearance of the Ge–H stretching mode. Dotted lines indicate the Nernst slope of 59 mV/pH. (b) Peak centers of components found by SVD-based deconvolution. Symbols ν_{high} and ν_{low} refer to the potential dependent higher and lower, respectively, wavenumber main component at the respective pH.

surface transformation related species, as these occur at the same potentials.

IV. SUMMARY AND CONCLUSION

The pH dependence of the electrode potential triggered desolvation of Ge(100) was investigated in perchlorate electrolytes in the pH range 1–10. CVs show the expected pH dependence of the reductive peak indicating the surface transformation of ≈60 mV per pH unit. An SVD-based deconvolution technique of ATR-IR spectra, in which the different components were fitted to a sigmoidal dependence on electrode potential showed the loss in OH stretching mode absorbance during the surface transformation to be a two-stage process. Comparing the ATR-IR difference spectra to spectra of bulk water yielded the extraction of pH-dependent effective thicknesses of an equivalent desolvated layer at the Ge(100)/electrolyte interface. At the lowest electrode potential –0.99 V, these "hydrophobic gaps" were found to be typically 2–3 Å. The largest gap thicknesses were consistently observed at pH 5.9, i.e., near neutral pH. Analysis of the interfacial IR spectra shows a loss of strongly hydrogen-bound interfacial water at potentials negative to the surface transformation on germanium, an increase in the amount of water in the average bulk hydrogen bonding state, and an increase of free OH groups near the surface. Qualitatively, the trends are similar throughout the pH range investigated, with the expected shift in potentials with pH. The most surprising result in this study is strong changes in the spectra at low wavenumbers with potential near neutral pH. These are manifested in a strongly increasing baseline at wavenumbers below 1000 cm^{-1}. Experiments with D_2O-based electrolytes indicate that besides free carrier absorption, the onset of the librational modes of water contributes to these changes. Consequently, these changes indicate significant changes in the water structure. A detailed analysis and interpretation of these changes requires the recording of spectra in the far-IR range, and a combination of spectra data with *ab initio* calculations, and reflects a challenging field of further work.

ACKNOWLEDGMENTS

This work is supported by the Cluster of Excellence RESOLV (No. EXC 1069) funded by the Deutsche Forschungsgemeinschaft within the framework of the German Excellence Initiative. M.R. acknowledges funding by the European Union's Horizon 2020 research and innovation programme under the Marie Skłodowska-Curie Grant Agreement No. 705857. The authors acknowledge the MPIE machine shop for building the *in situ* experiment cells, Petra Ebbinghaus for technical assistance, as well as Lei Yang and Stefan Wippermann for helpful discussions. A.E. thanks M. Stratmann for continuous support.

[1] R. W. Gurney, *Ionic Processes in Solution* (McGraw-Hill, New York, 1953).
[2] K. D. Collins and M. W. Washabaugh, Q. Rev. Biophys. **18**, 323–422 (1985).
[3] D. T. Richens, *The Chemistry of Aqua Ions: Synthesis, Structure and Reactivity: A Tour Through the Periodic Table of the Elements* (Wiley, New York, 1997).
[4] H. S. Frank and M. W. Evans, J. Chem. Phys. **13**, 507 (1945).
[5] W. Blokzijl and J. B. F. N. Engberts, Angew. Chem., Int. Ed. Engl. **32**, 1545 (1993).
[6] N. T. Southall, K. A. Dill, and A. D. J. Haymet, J. Phys. Chem. B **106**, 521 (2002).
[7] M. Mucha, T. Frigato, L. M. Levering, H. C. Allen, D. J. Tobias, L. X. Dang, and P. Jungwirth, J. Phys. Chem. B **109**, 7617 (2005).
[8] C. Lee, J. A. McCammon, and P. J. Rossky, J. Chem. Phys. **80**, 4448 (1984).
[9] P. Jungwirth and D. J. Tobias, J. Phys. Chem. B **106**, 6361 (2002).
[10] T. Hotta, A. Kimura, and M. Sasai, J. Phys. Chem. B **109**, 18600 (2005).
[11] T. Ishiyama and A. Morita, J. Phys. Chem. C **111**, 721 (2007).
[12] D. B. Asay, M. T. Dugger, and S. H. Kim, Tribol. Lett. **29**, 67 (2008).
[13] W. Stumm, *Chemistry of the Solid-Water Interface: Processes at the Mineral-Water and Particle-Water Interface in Natural Systems* (Wiley, New York, 1992), pp. 157–162.
[14] Y.-J. Feng, A. Gago, L. Timperman, and N. Alonso-Vante, Electrochim. Acta **56**, 1009 (2011).
[15] K. P. Gong, F. Du, Z. H. Xia, M. Durstock, and L. M. Dai, Science **323**, 760 (2009).
[16] J. W. Schultze and A. W. Hassel, "Passivity of metals, alloys, and semiconductors," in *Encyclopedia of Electrochemistry*, edited by A. Bard, M. Stratmann, and G. Frankel (Wiley-VCH, Weinheim, 2003), Vol. 4, pp. 460–490.
[17] K. Bohnenkamp and H. Engell, Z. Elektrochem. **61**, 1184 (1957).
[18] J.-N. Chazalviel, A. Belaïdi, M. Safi, F. Maroun, B. Erné, and F. Ozanam, Electrochim. Acta **45**, 3205 (2000).
[19] R. Memming and G. Neumann, J. Electroanal. Chem. Interfacial Electrochem. **21**, 295 (1969).
[20] H. Gerischer and W. Mindt, Surf. Sci. **4**, 440 (1966).
[21] S. Nayak and A. Erbe, Phys. Chem. Chem. Phys. **18**, 25100 (2016).
[22] F. Maroun, F. Ozanam, and J.-N. Chazalviel, J. Phys. Chem. B **103**, 5280 (1999).

[23]F. E. G. Güner, J. Wåhlin, M. Hinge, and S. Kjelstrup, Chem. Phys. Lett. **622**, 15 (2015).
[24]P. Fenter and S. S. Lee, MRS Bull. **39**, 1056 (2014).
[25]M. Mezger, H. Reichert, S. Schöder, J. Okasinski, H. Schröder, H. Dosch, D. Palms, J. Ralston, and V. Honkimäki, Proc. Natl. Acad. Sci. U. S. A. **103**, 18401 (2006).
[26]M. Mezger, S. Schöder, H. Reichert, H. Schröder, J. Okasinski, V. Honkimäki, J. Ralston, J. Bilgram, R. Roth, and H. Dosch, J. Chem. Phys. **128**, 244705 (2008).
[27]M. Sovago, R. K. Campen, G. W. H. Wurpel, M. Müller, H. J. Bakker, and M. Bonn, Phys. Rev. Lett. **100**, 173901 (2008).
[28]C. S. Tian and Y. R. Shen, Proc. Natl. Acad. Sci. U. S. A. **106**, 15148 (2009).
[29]O. Teschke and E. F. de Souza, Chem. Phys. Lett. **403**, 95 (2005).
[30]O. Teschke and E. F. de Souza, Phys. Chem. Chem. Phys. **7**, 3856 (2005).
[31]N. Kitadai, T. Sawai, R. Tonoue, S. Nakashima, M. Katsura, and K. Fukushi, J. Solution Chem. **43**, 1055 (2014).
[32]G. E. Ewing, J. Phys. Chem. B **108**, 15953 (2004).
[33]Q. Du, E. Freysz, and Y. R. Shen, Science **264**, 826 (1994).
[34]T. A. Weber and F. H. Stillinger, J. Phys. Chem. **87**, 4277 (1983).
[35]P. A. Thiel, F. M. Hoffmann, and W. H. Weinberg, J. Chem. Phys. **75**, 5556 (1981).
[36]B. Maté, A. Medialdea, M. A. Moreno, R. Escribano, and V. J. Herrero, J. Phys. Chem. B **107**, 11098 (2003).
[37]M. Nakamura, Y. Shingaya, and M. Ito, Chem. Phys. Lett. **309**, 123 (1999).
[38]B. W. Callen, K. Griffiths, and P. R. Norton, Phys. Rev. Lett. **66**, 1634 (1991).
[39]W. Gan, D. Wu, Z. Zhang, R. R. Feng, and H. F. Wang, J. Chem. Phys. **124**, 114705 (2006).
[40]D. A. Schmidt and K. Miki, J. Phys. Chem. A **111**, 10119 (2007).
[41]L. F. Scatena, M. G. Brown, and G. L. Richmond, Science **292**, 908 (2001).
[42]F. Niu, R. Schulz, A. Castañeda Medina, R. Schmid, and A. Erbe, Phys. Chem. Chem. Phys. **19**, 13585 (2017).
[43]M. Rabe, H. R. Zope, and A. Kros, Langmuir **31**, 9953 (2015).
[44]S. Nayak, P. U. Biedermann, M. Stratmann, and A. Erbe, Phys. Chem. Chem. Phys. **15**, 5771 (2013).
[45]S. Nayak, P. U. Biedermann, M. Stratmann, and A. Erbe, Electrochim. Acta **106**, 472 (2013).
[46]See https://edmond.mpdl.mpg.de/imeji/collection/Tr6mbX98OcP9_C0J for "Data package for: Vibrational spectroscopic study of pH dependent solvation at an Ge(100)-water interface during an electrode potential triggered surface termination transition," 2018.
[47]R. I. Shrager, Chemom. Intell. Lab. Syst. **1**, 59 (1986).
[48]R. W. Hendler and R. I. Shrager, J. Biochem. Biophys. Methods **28**, 1 (1994).
[49]F. Maroun, J.-N. Chazalviel, F. Ozanam, and D. Lincot, J. Electroanal. Chem. **549**, 161 (2003).
[50]J. P. Hoare, J. Electrochem. Soc. **116**, 1168 (1969).
[51]N. Wiberg, *Hollemann-Wiberg, Lehrbuch der Anorganischen Chemie*, 101st ed. (Walter de Gruyter, Berlin, 1995), p. 958.
[52]M. Cardona, Phys. Status Solidi B **118**, 463 (1983).
[53]S. Rivillon, Y. J. Chabal, F. Amy, and A. Kahn, Appl. Phys. Lett. **87**, 253101 (2005).
[54]E. Crowell and G. Lu, J. Electron Spectrosc. Relat. Phenom. **54-55**, 1045 (1990).
[55]F. Maroun, F. Ozanam, and J.-N. Chazalviel, Surf. Sci. **427-428**, 184 (1999).
[56]C. I. Ratcliffe and D. E. Irish, Can. J. Chem. **62**, 1134 (1984).
[57]L. Bencivenni, R. Caminiti, A. Feltrin, F. Ramondo, and C. Sadun, J. Mol. Struct.: THEOCHEM **257**, 369 (1992).
[58]A. Karelin, Z. Grigorovich, and V. Rosolovskii, Spectrochim. Acta, Part A **31**, 765 (1975).
[59]H. Gobrecht, A. De Haan, and R. Thull, Ber. Bunsen-Ges. Phys. Chem. **76**, 602 (1972).
[60]C. Bohren and D. R. Huffman, *Absorption and Scattering of Light by Small Particles* (Wiley, New York, 1983).
[61]W. Kaiser, R. J. Collins, and H. Y. Fan, Phys. Rev. **91**, 1380 (1953).
[62]E. Kane, J. Phys. Chem. Solids **1**, 82 (1956).
[63]A. H. Kahn, Phys. Rev. **97**, 1647 (1955).
[64]J. Bertie and Z. Lan, Appl. Spectrosc. **50**, 1047 (1996).
[65]A. Erbe, A. Sarfraz, C. Toparli, K. Schwenzfeier, and F. Niu, in *Soft Matter at Aqueous Interfaces*, Volume 917 of Lecture Notes in Physics, edited by P. R. Lang and Y. Liu (Springer, Cham, Switzerland, 2016), pp. 459–490.
[66]H. R. Zelsmann, J. Mol. Struct. **350**, 95 (1995).
[67]R. Khatib, T. Hasegawa, M. Sulpizi, E. H. G. Backus, M. Bonn, and Y. Nagata, J. Phys. Chem. C **120**, 18665 (2016).
[68]Y. Maréchal, J. Mol. Struct. **1004**, 146 (2011).
[69]N. J. Harrick, *Internal Reflection Spectroscopy* (Harrick Scientific, New York, 1987).
[70]M. Falk and T. A. Ford, Can. J. Chem. **44**, 1699 (1966).
[71]M. Schubert, Phys. Rev. B **53**, 4265 (1996).
[72]M. Reithmeier and A. Erbe, Phys. Chem. Chem. Phys. **12**, 14798 (2010).
[73]D. B. Asay and S. H. Kim, J. Phys. Chem. B **109**, 16760 (2005).
[74]M. Foster, M. Furse, and D. Passno, Surf. Sci. **502-503**, 102 (2002).
[75]M. Foster, M. D'Agostino, and D. Passno, Surf. Sci. **590**, 31 (2005).
[76]P. B. Miranda, L. Xu, Y. R. Shen, and M. Salmeron, Phys. Rev. Lett. **81**, 5876 (1998).
[77]M. S. Bergren, D. Schuh, M. G. Sceats, and S. A. Rice, J. Chem. Phys. **69**, 3477 (1978).
[78]J. Janeček and R. R. Netz, Langmuir **23**, 8417 (2007).
[79]Q. Du, R. Superfine, E. Freysz, and Y. R. Shen, Phys. Rev. Lett. **70**, 2313 (1993).
[80]A. Yamakata, E. Soeta, T. Ishiyama, M. Osawa, and A. Morita, J. Am. Chem. Soc. **135**, 15033 (2013).
[81]L. F. Scatena and G. L. Richmond, J. Phys. Chem. B **105**, 11240 (2001).
[82]M. G. Brown, D. S. Walker, E. A. Raymond, and G. L. Richmond, J. Phys. Chem. B **107**, 237 (2003).
[83]S. Devineau, K. I. Inoue, R. Kusaka, S. H. Urashima, S. Nihonyanagi, D. Baigl, A. Tsuneshige, and T. Tahara, Phys. Chem. Chem. Phys. **19**, 10292 (2017).
[84]M. A. Sánchez, T. Kling, T. Ishiyama, M.-J. van Zadel, P. J. Bisson, M. Mezger, M. N. Jochum, J. D. Cyran, W. J. Smit, H. J. Bakker, M. J. Shultz, A. Morita, D. Donadio, Y. Nagata, M. Bonn, and E. H. G. Backus, Proc. Natl. Acad. Sci. U. S. A. **114**, 227 (2017).